Cation distributions estimated using the magnetic moments of the spinel ferrites $Co_{1-x}Cr_xFe_2O_4$ at 10 K*

Shang Zhi-Feng(尚志丰)[a], Qi Wei-Hua(齐伟华)[a], Ji Deng-Hui(纪登辉)[a)b)], Xu Jing(徐 静)[a], Tang Gui-De(唐贵德)[a)†], Zhang Xiao-Yun(张晓云)[a], Li Zhuang-Zhi(李壮志)[a], and Lang Li-Li(郎莉莉)[a]

[a] *Hebei Advanced Thin Film Laboratory, Department of Physics, Hebei Normal University, Shijiazhuang* 050024, *China*
[b] *Department of Physics and Electronic Science, Liupanshui Normal University, Liupanshui* 553004, *China*

(Received 14 January 2014; revised manuscript received 14 April 2014; published online 10 August 2014)

$(A)[B]_2O_4$ ferrite samples with the composition $Co_{1-x}Cr_xFe_2O_4$ ($0.0 \le x \le 1.0$) are prepared using a hydrothermal method, and subjected to calcining in a tube furnace with an argon-flow at 1673 K for 2 h. X-ray diffraction patterns indicate that each of all the samples has a single phase cubic spinel structure with a space group of $Fd\bar{3}m$. Magnetic measurements show that the saturation magnetization decreases with as the Cr content x increases. The cation distribution of the samples is estimated by fitting the dependence of the magnetic moments on x at 10 K, using the quantum mechanical model previously proposed by our group. The calculated sum of the content values of the Cr^{3+} and Cr^{2+} cations occupying the (A) sites increases as the value of x increases. In the fitting process, the magnetic moment directions of the Cr^{3+} and Cr^{2+} cations are assumed to be antiparallel to those of the Fe and Co cations, respectively, which is in accordance with Hund's rules.

Keywords: spinel ferrite, magnetic property, cation distribution, ionicity

PACS: 75.75.–c, 81.40.Rs **DOI:** 10.1088/1674-1056/23/10/107503

1. Introduction

Co ferrites with striking magnetic, electrical, and optical properties have potential applications in various fields, such as recording tapes, permanent magnets, hard disc recording media, read-write heads, magnetic drug delivery, catalysis, color imaging, magnetic refrigeration, magnetic resonance imaging (MRI) contrast enhancement, magnetic cell separation, etc.[1–5] $CoFe_2O_4$ is a typical spinel ferrite with an $(A)[B]_2O_4$ structure. Each spinel unit cell contains eight formula units. The large oxygen anions form a close-packed face-centered-cubic structure with the smaller metal cations occupying the interstitial positions. There are two types of interstitial sites occupied by the metal cations: the tetrahedral (8*a*) or (A) sites, and the octahedral (16*d*) or [B] sites.[6,7] In the traditional theory, $CoFe_2O_4$ has an inverse spinel structure where 8 Fe^{3+} cations occupy the (A) sites, the other 8 Fe^{3+} cations and the 8 Co^{2+} cations occupy [B] sites. The cation magnetic moments at the [B] sites are parallel at low temperature, due to the fact that the itinerant electrons, with a constant spin direction, hop between neighboring cations mediated by O2p electrons. However, the cation moments at the (A) sites are antiparallel to those at the [B] sites, due to the superexchange interaction between cations at the (A) sites and cations at the [B] sites, which is mediated by oxygen anions.[6–8]

The spinel structure allows the introduction of different metallic ions, which can change the magnetic properties considerably. However, there are obvious discrepancies for the Cr cation distribution in the spinel ferrites, as reported previously in some papers, such as Refs. [9]–[15]. Cojocariu *et al.*[9] prepared samples of $CoFe_2O_4$ and $CoCr_{0.2}Fe_{1.8}O_4$. They thought that all Cr cations entered into the [B] sites and that some of the Co cations migrated to the (A) sites from the [B] sites, resulting in cation distributions in the form of $(Co_{0.05}Fe_{0.95})[Co_{0.95}Fe_{1.05}]O_4$ and $(Co_{0.17}Fe_{0.83})[Co_{0.83}Cr_{0.2}Fe_{0.97}]O_4$. Chae *et al.*[10] thought that all Cr cations entered into the [B] sites, while some of the Co cations migrated to the [B] sites from the (A) sites, resulting in cation distributions in the form of $(Co_{0.65}Fe_{0.35})[Co_{0.35}Fe_{1.65}]O_4$ and $(Co_{0.33}Fe_{0.67})[Co_{0.67}Cr_{0.2}Fe_{1.13}]O_4$. Magalhães *et al.*[14] prepared a series of Cr-containing magnetites, $Fe_{3-x}Cr_xO_4$ ($x =$ 0.00, 0.07, 0.26, 0.42, and 0.51) by using a conventional co-precipitation method. By using Mössbauer spectroscopy and powder X-ray diffraction measurements, they determined that the samples had spinel crystalline phases, in which only Fe^{3+}_{oct} ([B] sites) ions were substituted by Cr^{3+} when there was a low Cr concentration, and both Fe^{2+}_{oct} ([B] sites) and Fe^{3+}_{tet} ((A) sites) ions were substituted by chromium ions for higher Cr concentrations. Yunus *et al.*[15] prepared samples of $Ga_xCoCrFe_{1-x}O_4$ ($0.0 \le x \le 1.0$). On the basis of the analysis of neutron diffraction, they thought that a portion of the Cr cations migrated to the (A) sites from the [B] sites due to doping with the Ga cations. However, the sample magnetic

*Project supported by the National Natural Science Foundation of China (Grant No. NSF-11174069), the Natural Science Foundation of Hebei Province, China (Grant No. E2011205083), the Key Item Science Foundation of the Education Department of Hebei Province, China (Grant No. ZD2010129), and the Young Scholar Science Foundation of the Education Department of Hebei Province, China (Grant No. QN20131008).

†Corresponding author. E-mail: tanggd@mail.hebtu.edu.cn

© 2014 Chinese Physical Society and IOP Publishing Ltd

moments they calculated using their cation distributions were significantly higher than the corresponding experimental values. Given the conflicting results obtained in these systems, it is clear that the Cr cation distribution in the spinel ferrites requires to be further investigated.

In previous reports, we proposed a quantum-mechanical potential barrier model for estimating the cation distribution in spinel ferrites.[16–19] We then proposed a method of estimating the ionicity of spinel ferrites[20] by comparing with the method from Phillips.[21] On the basis of these studies, we estimated the cation distributions in the spinel ferrites $Co_{1+x}Fe_{2-x}O_4$ ($0.0 \leq x \leq 2.0$) by using the magnetic moments of the samples at 10 K.[22] The Co ion content values at the (A) sites that we estimated are close to the corresponding experimental results reported by Ferreira *et al*., who used the Mössbauer spectra.[23]

For the spinel ferrite samples $Cr_xFe_{3-x}O_4$ ($0.0 \leq x \leq 1.0$), the assumption that the magnetic moments of Cr^{2+} and Cr^{3+} cations are antiparallel to those of the Fe cations in the samples was made,[24] and the dependence of the cation distribution on the Cr doping was estimated by using a method similar to that of Ref. [22]. We then estimated the cation distribution on the basis of the dependence of the saturation magnetization of $NiCr_xFe_{2-x}O_4$ ($0.0 \leq x \leq 1.0$) at 10 K on Cr doping level x.[25] The estimated concentration of Cr cations at the (A) sites increased with increasing Cr doping level x, and the concentrations were found to be close to the experimental results from neutron diffraction, as reported by Ghatage *et al*.[26]

In this paper, we prepare the spinel ferrite samples $Co_{1-x}Cr_xFe_2O_4$ ($0.0 \leq x \leq 1.0$), and estimate, on the basis of our previous work,[17,18,24,25] the cation distribution by fitting the dependence of the saturation magnetization at 10 K, on the Cr doping level. Our estimated Co cation content at the (A) sites in the sample $CoFe_2O_4$ ($x = 0.0$) is 0.24, resulting in the structure $(Co_{0.24}Fe_{0.76})[Co_{0.76}Fe_{1.24}]O_4$. We note that the value 0.24 lies between the values 0.05 and 0.65 obtained by Cojocariu *et al*.[9] and Chae *et al*.,[10] respectively. It is also noteworthy that our estimated Cr cation content at the (A) sites increases with increasing the Cr doping level x, up to 0.36 when $x = 1.0$. This tendency is similar to those of the experimental results for the samples $NiCr_xFe_{2-x}O_4$ ($0.0 \leq x \leq 1.0$) obtained from the neutron diffraction results reported by Ghatage *et al*.[26]

2. Experiment

2.1. Sample preparation

Ferrite powder samples $Co_{1-x}Cr_xFe_2O_4$ ($0.0 \leq x \leq 1.0$) were prepared by a hydrothermal method. The chemicals used for synthesizing the cobalt ferrite were cobalt nitrate ($Co(NO_3)_2{\cdot}6H_2O$), iron nitrate ($Fe(NO_3)_3{\cdot}9H_2O$), chromium chloride ($CrCl_3{\cdot}6H_2O$), and sodium hydroxide (NaOH). All of these chemicals were of analytical grade. The hydrothermal reactions were carried out in a stainless-steel autoclave with a teflon liner (150-ml total capacity) under autogenous pressure. In the synthesis process, the metal salts were taken in stoichiometric ratios for each value of x and dissolved in 40-ml deionized water. The solutions were stirred at a constant temperature of 343 K. The the pH value of the solution was adjusted to 11.0 by adding 3-molar NaOH solutions, drop-by-drop, and then stirring for 30 min. A homogeneous solution was obtained. The solution was transferred into the autoclave. The autoclave was sealed and maintained at 423 K for 24 h. The resulting products were then washed several times with deionized water to remove the Na^+, NO_3^-, and Cl^- ions. A black precipitate was collected by filtration, and dried in air for 24 h at 363 K, and then for 24 h at 423 K in a drying cabinet. The dried precipitate was ground in an agate mortar for 30 min to obtain a fine powder, and then calcined for 2 h at 1673 K in a tube furnace with argon flow. The final samples were obtained after 30-min grinding, again in the agate mortar.

2.2. Sample characterization

The crystal structures of the samples were identified by X-ray diffraction (XRD) using an X'pert Pro X-ray diffractometer with Cu K_α ($\lambda = 1.5406$ Å) radiation at room temperature. The data were collected in a 2θ range of 15°–120° in steps of 0.01671°. Micrographs of the particles in the samples were observed using an S-4800 scanning electron microscope (SEM). The composition of the samples was analyzed through the X-ray energy-dispersive spectrum (EDS), which was obtained using an INCA PentaFETx3 system, with an accelerating voltage of 20 kV. The magnetization measurements were performed using a vibrating sample magnetometer (VSM, Quantum Design Corporation, PPMS, USA, 9T) in an external field of up to 3 T at temperatures of 10 K and 300 K.

3. Results and discussion

3.1. Structural analysis

The X-ray diffraction (XRD) patterns for the samples $Co_{1-x}Cr_xFe_2O_4$ ($0.0 \leq x \leq 1.0$) are shown in Fig. 1, and indicate the presence of a single phase, cubic spinel structure with a space group $Fd\bar{3}m$. The X-ray diffraction pattern data for the samples are fitted by using the Rietveld powder diffraction profile fitting technique[27] using the X'Pert HighScore Plus software. The Rietveld fitting parameters for the samples are listed in Table 1. It can be seen that the various error parameters, the profile factor, R_p, the weighted profile factor, R_{wp}, and the goodness of fit indicator, s, are all acceptable. The

crystal lattice constant a, the distances from the O anion to the cations at the (A) and [B] sites, d_{AO} and d_{BO}, the distance from the cations at the (A) sites to those at the [B] sites, d_{AB}, as obtained in the fitting process are also listed in Table 1. For the cubic spinel structure, the ideal values of d_{AO}, d_{BO}, and d_{AB} are $\sqrt{3}a/8$, $a/4$, and $\sqrt{11}a/8$. However, for all of our samples, the observed values of d_{AO} and d_{BO} in Table 1 are 1.066 and 0.968 times the ideal values, respectively, while the value of d_{AB} is equal to its ideal value; that is,

$$d_{AO} = 1.066 \times \frac{\sqrt{3}}{8}a, \quad d_{BO} = 0.968 \times \frac{1}{4}a, \quad d_{AB} = \frac{\sqrt{11}}{8}a. \quad (1)$$

Figure 2 shows the variation of crystal lattice constant with Cr-doping level x. It can be seen that there is a minimum value of the crystal lattice constant when $x = 0.4$. A reasonable representation of the variation of the lattice constant a with Cr concentration x can be given in the form of two straight lines intersecting at $x = 0.4$:

$$\begin{aligned} a &= 8.3840 - 0.0582x, \quad (x \le 0.4), \\ a &= 8.3370 + 0.0588x, \quad (x > 0.4). \end{aligned} \quad (2)$$

This variation of the lattice constant will be discussed in Subsection 3.6.

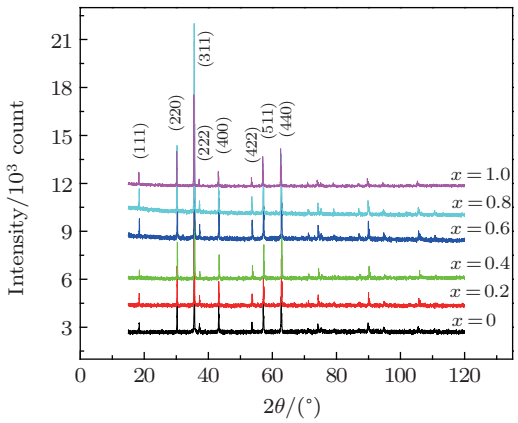


Fig. 1. (color online) X-ray diffraction patterns for the samples $Co_{1-x}Cr_xFe_2O_4$ ($0.0 \le x \le 1.0$).

The results from the X'Pert HighScore Plus software also indicate that the volume-averaged diameter of the crystallites in all of the samples is larger than 100 nm, so that the surface effects of the crystallites are expected to be very weak in all of the samples.

Table 1. Rietveld fitted results for the XRD diffraction patterns of the samples $Co_{1-x}Cr_xFe_2O_4$ ($0.0 \le x \le 1.0$), where s, R_p, and R_{wp} are the goodness of fit indicator, profile factor, and weighted profile factor, respectively; a is the lattice parameter; d_{AO} and d_{BO} are the distances from the O anion to the cations at the (A) and [B] sites, respectively; d_{AB} is the distance from the cations at the (A) sites to those at the [B] sites.

x	a/Å	d_{AO}/Å	d_{BO}/Å	d_{AB}/Å	s	R_p/%	R_{wp}/%
0.0	8.385	1.936	2.029	3.476	0.96	1.43	1.91
0.2	8.371	1.933	2.026	3.470	0.95	1.54	2.09
0.4	8.361	1.930	2.023	3.466	1.02	1.76	2.30
0.6	8.380	1.935	2.028	3.474	1.13	1.53	1.86
0.8	8.383	1.935	2.029	3.475	1.27	1.85	2.13
1.0	8.394	1.938	2.031	3.480	1.27	2.93	3.37

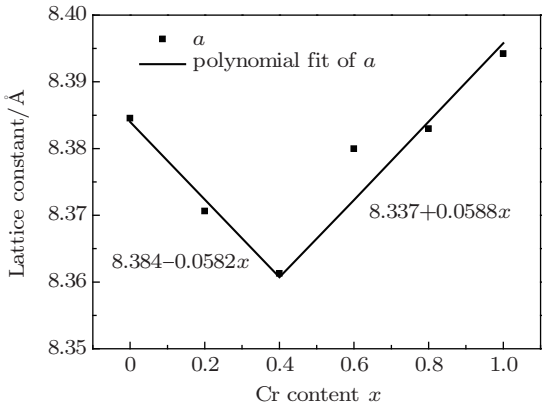


Fig. 2. Variation of the crystal lattice constant with Cr-doping level x in $Co_{1-x}Cr_xFe_2O_4$ ($0.0 \le x \le 1.0$).

3.2. Scanning electron microscopy analysis

Scanning electron micrographs of the $Co_{1-x}Cr_xFe_2O_4$ ($0.0 \le x \le 1.0$) samples are shown in Fig. 3. From Figs. 3(c)–3(e), it may be seen that the particles are octahedral with sizes of about 0.5 μm–2 μm. Therefore, these samples are monocrystal powders. In Figs. 3(a), 3(b), and 3(f), there are no distinct octahedral particles, indicating that these samples are polycrystal powders.

3.3. X-ray energy dispersive spectrum analysis

The X-ray energy dispersive spectra (EDS) of the samples are shown Fig. 4(a), from which the content values of various elements in the samples may be determined. The results are shown in Fig. 4(b). It can be seen from Fig. 4(b) that the sample compositions measured by EDS (points) are very close to the nominal compositions (line). Therefore, the nominal compositions are used in the following discussion.

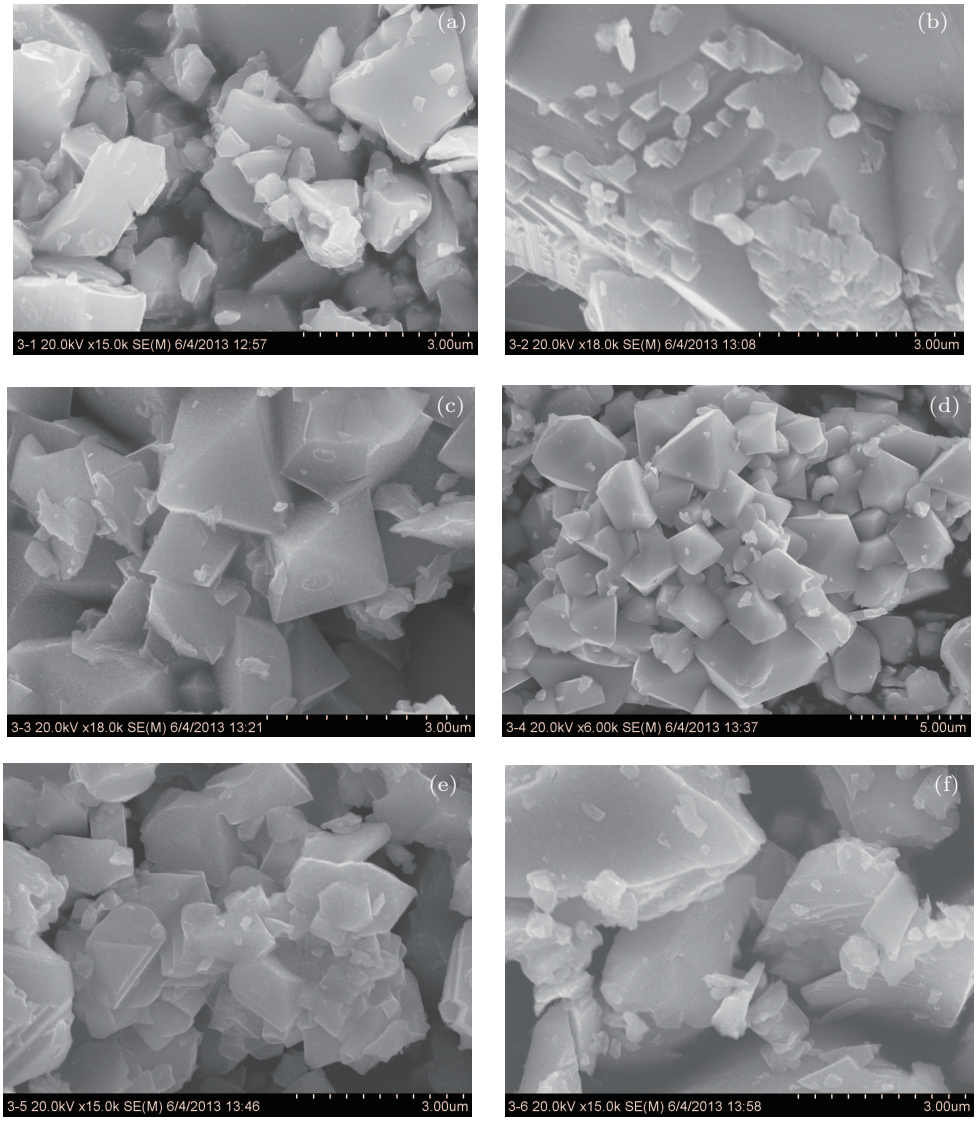


Fig. 3. Scanning electron micrographs of the samples $Co_{1-x}Cr_xFe_2O_4$: (a) $x = 0.0$, (b) $x = 0.2$, (c) $x = 0.4$, (d) $x = 0.6$, (e) $x = 0.8$, (f) $x = 1.0$.

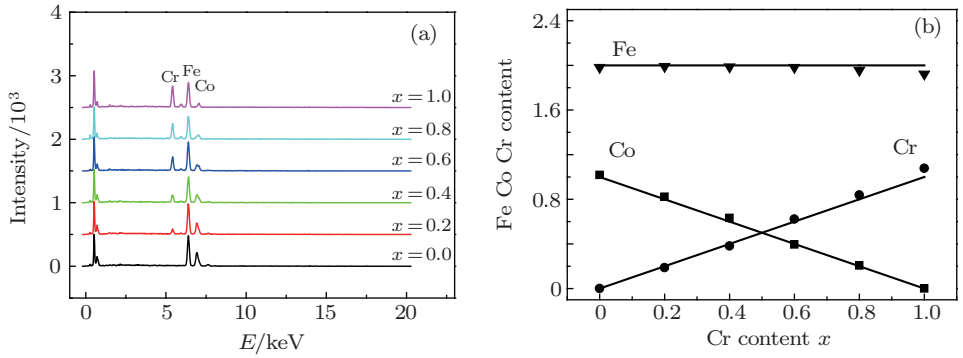


Fig. 4. (color online) (a) EDS patterns for the samples $Co_{1-x}Cr_xFe_2O_4$ ($0.0 \leq x \leq 1.0$); (b) the nominal content values (lines) and the observed values (points) from EDS for Co, Fe, and Cr.

3.4. Magnetic properties analysis

Figures 5(a) and 5(b) show the magnetic hysteresis loops for the samples $Co_{1-x}Cr_xFe_2O_4$ ($0.0 \leq x \leq 1.0$) measured at 10 K and 300 K. The specific saturation magnetization (σ_s), remanent magnetization (σ_r), and coercive field (H_c) of the samples at 10 K are listed in Table 2. It can be seen that σ_s decreases with increasing the Cr-doping level x at 10 K. In Table 2, μ_{exp} is the magnetic moment per formula of sample, calculated from σ_s at 10 K.

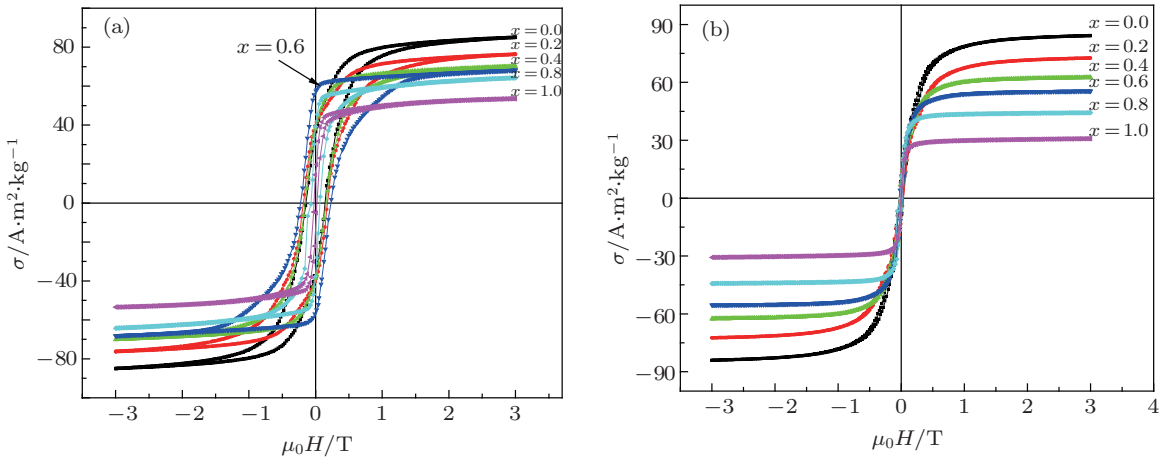


Fig. 5. (color online) Magnetic hysteresis loops for the samples $Co_{1-x}Cr_xFe_2O_4$ ($0.0 \leq x \leq 1.0$) measured at 10 K (a) and 300 K (b).

Table 2. Values of specific saturation magnetization σ_s, remanent magnetization σ_r, and coercive field $\mu_0 H_c$ for the samples $Co_{1-x}Cr_xFe_2O_4$ measured at 10 K. μ_{exp} is the magnetic moment per formula of sample, calculated from σ_s.

x	σ_s/(A·m^2/kg)	σ_r/(A·m^2/kg)	$\mu_0 H_c$/mT	$\mu_{exp}/(\mu_B$/formula)
0.0	81.25	35.09	1441	3.34
0.2	69.60	40.04	1824	3.02
0.4	60.35	38.41	1548	2.77
0.6	54.69	56.92	2257	2.63
0.8	43.43	38.62	672	2.44
1.0	29.89	15.54	210	2.04

3.5. Cation distribution and magnetic structure for $Co_{1-x}Cr_xFe_2O_4$ ($0.0 \leq x \leq 1.0$)

As pointed out in the Introduction, there are issues regarding the Cr cation distribution in the spinel ferrites. In our opinion, a very important characteristic of Cr cations, which is different from those of Fe, Co, Ni, and Cu, has been neglected in all previous reports: the numbers of 3d electrons in Cr^{3+} and Cr^{2+} are 3 and 4, respectively, which result in the magnetic moments of Cr cations being antiparallel to those of Fe in $Cr_xFe_{3-x}O_4$.[24]

In order to better understand the magnetic ordering mechanism of the ferrites $M_xFe_{3-x}O_4$ (M = Cr, Mn, Fe, Co, Ni, Cu; $0.0 \leq x \leq 1.0$), our group proposed a new magnetic ordering model,[24] in which three factors were considered simultaneously. Firstly, the O2p electrons serve as intermediaries for the itinerant 3d electrons between the cations; secondly, magnetic ordering in spinal ferrites is dependent on the number of 3d electrons, including local and the itinerant 3d electrons in the cations, subjected to constraints arising from Hund's rules; and, thirdly, the spin directions of the itinerant electrons remain constant in the hopping process between the cations. This can be understood as follows.

(i) There is a certain probability of finding 2p electrons with opposite spin directions in the outer orbits of the oxygen anions (taking into consideration the ionicity), which serve as intermediaries for the itinerant 3d electrons between the cations. Therefore, the metal cations around an oxygen anion are divided into two groups with opposite spin direction itinerant electrons. Those cations with the same bond lengths and bond angles between the oxygen anion and the metal cations will constitute a single group, in order to minimize the energy change of the system when the itinerant electron, with constant spin direction, hops between the cations. For example, the spin directions of itinerant electrons in the (A) sublattice is opposite to those in the [B] sublattice in spinel ferrites because the distance between cation and anion in the (A) sublattice is $\left(\sqrt{3}/8\right)a$, while the distance between the cation and anion in the [B] sublattice is $a/4$, where a is the lattice constant of the spinel unit cell.

(ii) In a group of metal cations, the spin direction of the itinerant electron remains constant when it moves to any cation and the spin directions of the 3d electrons (including itinerant and local 3d electrons) are constrained by Hund's rules. Hence, the directions of cation magnetic moments are determined.

By Hund's rules, the spins of electrons in a subshell of a free atom tend to align in one direction until the maximum multiplicity is attained. After that, the electron spins will align in the opposite direction. Thus, in the 3d subshell of free transition metal atoms, a maximum of five electrons can have their spins aligned in one direction.[28]

In $Co_{1-x}Cr_xFe_2O_4$ spinel ferrites, the 3d electron num-

bers of Cr^{3+}, Cr^{2+}, Fe^{3+}, Fe^{2+}, Co^{3+}, Co^{2+} cations are 3, 4, 5, 6, 6, 7, respectively. It is easy to see that the number, n_d, of 3d electrons in Cr^{3+} and Cr^{2+}, in that $n_d \leq 4$, differs from that of the other ions in that $n_d \geq 5$. Therefore, when an itinerant electron hops to a Cr^{3+} or Cr^{2+} cation in a spinel ferrite, the spin direction of this itinerant electron will be parallel to that of the local 3d electron (major spin). However, when an itinerant electron hops to an Fe or Co cation (with $n_d \geq 5$), the spin direction of this itinerant electron will be antiparallel to that of the local 3d electron (major spin). Thus, at the [B] sites [or (A) sites] of the spinel ferrite, the magnetic moment directions of Cr^{3+} and Cr^{2+} cations will be antiparallel to those of Fe and Co cations, due to the fact that the spin direction of the itinerant electron remains constant in the hopping process.

According to the quantum mechanical model proposed by our group[16–19] for estimating the cation distribution in spinel ferrites, there are three important factors that affect the cation distribution in spinel ferrites doped with magnetic cations.

Firstly, in an oxide, the probability with which a cation losses an electron should relate to the ionization energy of the electron and the distance from this cation to its adjacent oxygen anion. We estimate this by assuming that there is a square potential barrier between the cation and the anion in cation-anion pair. The height and width of the potential barrier relate to the ionization energy of the last ionized electron, as well as the distance between neighboring cations and anions. The probability ratio (R) of the different cations therefore relates to the probability of their last ionized electrons transmitting through the potential barrier, and takes the form,[16,17]

$$R = \frac{T_C}{T_D} = \frac{V_D}{V_C} \exp\left[10.24\left(r_D V_D^{1/2} - c r_C V_C^{1/2}\right)\right], \quad (3)$$

where nanometers (nm) and electron-volts (eV) are used as the units of length and energy; T_C (T_D) represents the probability with which the last ionized electron of the C (D) cations jumps to the anion through a potential barrier with height V_C (V_D) and width r_C (r_D); V_C and V_D are the ionization energies of last ionized electron of the cations C and D, respectively; and, r_C and r_D are the distances from the cations C and D to the anions, respectively. The parameter c is a barrier shape correcting constant relating to the extent to which the shapes of the two potential barriers deviate from a square barrier. It is obvious that parameter $c = 1$ when $V_C = V_D$ and $r_C = r_D$. In the following discussion, we let $c = 1$.

Secondly, the Pauli repulsion energy of the electron cloud between neighboring cations and anions must be considered. This can be taken into account by using the effective ionic radius:[29] smaller ions should be located at the sites with smaller available space in the lattice. For instance, the volumes of the (A) sites are smaller than those of the [B] sites in the spinel ferrites.

Thirdly, a tendency toward charge density balance forces a part of the M^{2+} ions (with large effective ionic radius) to enter into the (A) sites from the [B] sites (with larger available space) by jumping an equivalent potential barrier V_{BA} in the thermal treatment process prepared samples. The V_{BA} arises from the Pauli repulsion energy of the electron cloud as well as from the magnetic ordered energy. In addition, V_{BA} is related to the ionization energies.

In addition, due to the fact that there are both ionic and covalent bonds in oxides, it is useful to consider the ionicity defined as the fraction of ionic bonds.[21] A method to estimate ionicity for spinel ferrites was proposed by our group.[20] In Ref. [20], the calculated ionicity of Fe_3O_4 was found to be 0.8790, indicating that the total valence per formula is 7.032 and that the total number of trivalent cations per formula is 1.032, rather than 2.000 (from the traditional theory). We therefore consider that the ionicity of Fe is 0.8790 in spinel ferrites. Similarly, we also estimate the ionicities of Co and Cr in spinel ferrites, and obtain the values of 0.8314 and 0.8726, respectively.[20]

Subject to the above constraints, the cation distributions in the $Co_{1-x}Cr_xFe_2O_4$ ($0.0 \leq x \leq 1.0$) samples can be represented by the formula,

$$(Fe^{3+}_{y1}Cr^{3+}_{y2}Co^{3+}_{y3}Fe^{2+}_{y4}Cr^{2+}_{y5}Co^{2+}_{y6})[Fe^{2+}_{2-y1-y4-z1}Cr^{2+}_{x-y2-y5-z2}Co^{2+}_{1-x-y3-y6-z3}Fe^{3+}_{z1}Cr^{3+}_{z2}Co^{3+}_{z3}]O_4. \quad (4)$$

It can be seen from Eq. (2) that,

$$y_1 + y_2 + y_3 + y_4 + y_5 + y_6 = 1, \quad (5)$$

$$y_1 + y_2 + y_3 + z_1 + z_2 + z_3 = N_3, \quad (6)$$

where N_3 is the number of trivalent cations per formula and

$$N_3 = (8/3)[f_{Co}(1.0 - x) + f_{Cr}x + f_{Fe}2.0] - 6.0, \quad (7)$$

where f_{Co}, f_{Cr}, and f_{Fe}, which represent the ionicities of the Co, Cr, and Fe ions, are 0.8314, 0.8726, and 0.8790, respectively. Also, from Eq. (4), we have,

$$R_{A2}\frac{x}{2} = \frac{y_2}{y_1}, \quad R_{A3}\frac{1-x}{2} = \frac{y_3}{y_1}, \quad R_{A4} = \frac{y_4}{y_1},$$
$$R_{A5}\frac{x}{2} = \frac{y_5}{y_1}, \quad R_{A6}\frac{1-x}{2} = \frac{y_6}{y_1}, \quad (8)$$
$$R_{B2}\frac{x - y_2 - y_5}{2 - y_1 - y_4} = \frac{z_2}{z_1},$$
$$R_{B3}\frac{1 - x - y_3 - y_6}{2 - y_1 - y_4} = \frac{z_3}{z_1}. \quad (9)$$

The content ratios R_{A2}, R_{A3}, R_{A4}, R_{A5}, and R_{A6} of the Cr^{3+}, Co^{3+}, Fe^{2+}, Cr^{2+}, and Co^{2+} to the Fe^{3+} ions at the (A) sites, and the ratios R_{B2} and R_{B3} of the Cr^{3+} and Co^{3+} to the Fe^{3+} ions at [B] sites are discussed in what follows.

From Eqs. (5) and (8), we have,

$$y_1 = 2/[2+R_{A2}x+R_{A3}(1-x)+2R_{A4} +R_{A5}x+R_{A6}(1-x)]. \quad (10)$$

From Eqs. (6) and (9), we have the result that

$$z_1 = \frac{N_3-[1+0.5R_{A2}x+0.5R_{A3}(1-x)]y_1}{1+R_{B2}\cdot\dfrac{x-y_2-y_5}{2-y_1-y_4}+R_{B3}\cdot\dfrac{1-x-y_3-y_6}{2-y_1-y_4}}. \quad (11)$$

As indicated in the above discussion, the magnetic moment directions for Cr^{2+} ($n_d=4$) and Cr^{3+} ($n_d=3$) ions will be antiparallel to those of Fe^{3+} ($n_d=5$), Fe^{2+} ($n_d=6$), Co^{3+} ($n_d=6$), and Co^{2+} ($n_d=7$) in the same sublattice ([B] sublattice or (A) sublattice). Therefore, the magnetic moments of Cr^{3+}, Cr^{2+}, Fe^{3+}, Fe^{2+}, Co^{3+}, and Co^{2+} are represented by -3, -4, 5, 4, 4, and 3 μ_B. We can calculate the average magnetic moments per formula in samples of $Co_{1-x}Cr_xFe_2O_4$ ($0.0\le x\le 1.0$) from Eq. (4) to be

$$\begin{cases} \mu_C = \mu_{BT}-\mu_{AT}, \\ \mu_{AT} = 5y_1-3y_2+4y_3+4y_4-4y_5+3y_6, \\ \mu_{B1} = 4(2-y_1-y_4-z_1)+5z_1 \\ \qquad = 4(2-y_1-y_4)+z_1, \\ \mu_{B2} = -4(x-y_2-y_5-z_2)-3z_2 \\ \qquad = -4(x-y_2-y_5)+z_2, \\ \mu_{B3} = 3(1-x-y_3-y_6-z_3)+4z_3 \\ \qquad = 3(1-x-y_3-y_6)+z_3, \\ \mu_{BT} = \mu_{B1}+\mu_{B2}+\mu_{B3}, \end{cases} \quad (12)$$

where μ_{AT} and μ_{BT} are the magnetic moments of the (A) and [B] sublattices, respectively, and μ_{B1}, μ_{B2}, and μ_{B3} are the magnetic moments of Fe, Cr, and Co ions at the [B] sites, respectively.

By using the quantum mechanical model proposed by our group[17–20] to estimate the cation distribution in ferrites, the content ratios R_{A2}, R_{A3}, R_{A4}, R_{A5}, and R_{A6} of the Cr^{3+}, Co^{3+}, Fe^{2+}, Cr^{2+}, and Co^{2+} ions to the Fe^{3+} ions at the (A) sites, and the ratios R_{B2} and R_{B3} of the Cr^{3+} and Co^{3+} ions to the Fe^{3+} ions at the [B] sites, can be derived as

$$R_{A2} = \frac{T(Cr^{3+})}{T(Fe^{3+})} = \frac{V(Fe^{3+})}{V(Cr^{3+})} \times \exp\{10.24d_{AO}[V(Fe^{3+})^{1/2}-V(Cr^{3+})^{1/2}]\}, \quad (13)$$

$$R_{A3} = \frac{T(Co^{3+})}{T(Fe^{3+})} = \frac{V(Fe^{3+})}{V(Co^{3+})} \times \exp\{10.24d_{AO}[V(Fe^{3+})^{1/2}-V(Co^{3+})^{1/2}]\}, \quad (14)$$

$$R_{A4} = \frac{T(Fe^{2+})}{T(Fe^{3+})} = \frac{V(Fe^{3+})}{V(Fe^{2+})}\exp\{10.24[d_{AO}V(Fe^{3+})^{1/2} -d_{AO}V(Fe^{2+})^{1/2}-d_{AB}V_{BA}(Fe^{2+})^{1/2}]\}, \quad (15)$$

$$R_{A5} = \frac{T(Cr^{2+})}{T(Fe^{3+})} = \frac{V(Fe^{3+})}{V(Cr^{2+})}\exp\{10.24[d_{AO}V(Fe^{3+})^{1/2} -d_{AO}V(Cr^{2+})^{1/2}-d_{AB}V_{BA}(Cr^{2+})^{1/2}]\}, \quad (16)$$

$$R_{A6} = \frac{T(Co^{2+})}{T(Fe^{3+})} = \frac{V(Fe^{3+})}{V(Co^{2+})}\exp\{10.24[d_{AO}V(Fe^{3+})^{1/2} -d_{AO}V(Co^{2+})^{1/2}-d_{AB}V_{BA}(Co^{2+})^{1/2}]\}, \quad (17)$$

$$R_{B2} = \frac{T(Cr^{3+})}{T(Fe^{3+})} = \frac{V(Fe^{3+})}{V(Cr^{3+})} \times \exp\{10.24d_{BO}[V(Fe^{3+})^{1/2}-V(Cr^{3+})^{1/2}]\}, \quad (18)$$

$$R_{B3} = \frac{T(Co^{3+})}{T(Fe^{3+})} = \frac{V(Fe^{3+})}{V(Co^{3+})} \times \exp\{10.24d_{BO}[V(Fe^{3+})^{1/2}-V(Co^{3+})^{1/2}]\}. \quad (19)$$

Here, $V(Fe^{2+})=16.18$ eV, $V(Co^{2+})=17.06$ eV, $V(Cr^{2+})=15.50$ eV, $V(Fe^{3+})=30.65$ eV, $V(Co^{3+})=33.5$ eV, and $V(Cr^{3+})=30.96$ eV are the second and third ionization energies of Fe, Co, and Cr, respectively. The distances from the anion to cations at the (A) sites and the [B] sites, d_{AO} and d_{BO}, and the distance between the cations at the (A) sites and the [B] sites, d_{AB}, are the observed values in Table 1 derived from XRD patterns. Finally, $V_{BA}(Fe^{2+})$, $V_{BA}(Cr^{2+})$, and $V_{BA}(Co^{2+})$ are the heights of the equivalent potential barriers, each with width d_{AB}, which must be jumped over by the Fe^{2+}, Cr^{2+}, and Co^{2+} ions from the [B] to the (A) sites.

Because it is difficult for a divalent cation with a high ionization energy and large effective radius to enter into the (A) sites, we assume that

$$V_{BA}(Co^{2+}) = V_{BA}(Cr^{2+})\cdot V(Co^{2+})\cdot r(Co^{2+})/[V(Cr^{2+})\cdot r(Cr^{2+})], \quad (20)$$

$$V_{BA}(Fe^{2+}) = V_{BA}(Cr^{2+})\cdot V(Fe^{2+})\cdot r(Fe^{2+})/[V(Cr^{2+})\cdot r(Cr^{2+})], \quad (21)$$

where $r(Cr^{2+})$, $r(Co^{2+})$, and $r(Fe^{2+})$ are the effective radii of the Cr^{2+}, Co^{2+}, and Fe^{2+} cations, respectively.[29]

There are 20 independent expressions in Eqs. (5)–(9) and Eq. (12)–(21) for each Cr-doping level x. However, there are 21 parameters altogether: y_1–y_6, z_1–z_3, N_3, R_{A2}, R_{A3}, R_{A4}, R_{A5} and R_{A6}, R_{B2} and R_{B3}, $V_{BA}(Fe^{2+})$, $V_{BA}(Cr^{2+})$, and $V_{BA}(Co^{2+})$, and μ_C. Therefore, we need to obtain a value for at least one parameter in order to solve or fit the system of equations. The most direct approach is to fit experimental data for the magnetic moments. We also assume that $V_{BA}(Cr^{2+})$ varies linearly with increasing the Cr-doped level x, we then have only two independent parameters in the set of all the $V_{BA}(Fe^{2+})$, $V_{BA}(Cr^{2+})$, and $V_{BA}(Co^{2+})$ for $0.0\le x\le 1.0$. In this manner, if we can obtain the values of $V_{BA}(Cr^{2+})$ at $x=0.2$ and $x=0.8$, then we can calculate all of the other values of $V_{BA}(Co^{2+})$ and $V_{BA}(Fe^{2+})$ by using Eqs. (20) and (21).

By using the above equations and parameters to fit the observed magnetic moment values of the samples at 10 K, we obtain the values of $V_{BA}(Cr^{2+})$ of the samples $x = 0.2$ and $x = 0.8$ to be 1.146 eV and 0.932 eV, respectively. This allows us to obtain all other values of parameters $V_{BA}(Cr^{2+})$, $V_{BA}(Co^{2+})$, and $V_{BA}(Fe^{2+})$, the dependence on the Cr-doping level of the magnetic moments, and the cation distributions for $Co_{1-x}Cr_xFe_2O_4$ $(0.0 \le x \le 1.0)$ as shown in Table 3.

Table 3. Fitted results for the dependence on the Cr content of the cation distributions and the fitted magnetic moments μ_C of the samples. $V_{BA}(Fe^{2+})$, $V_{BA}(Cr^{2+})$, and $V_{BA}(Co^{2+})$ are the heights of the equivalent potential barriers which must be jumped over by the Fe^{2+}, Cr^{2+}, and Co^{2+} ions from the [B] to the (A) sites. N_3 is the total concentration of trivalent ions.

x	0.0	0.2	0.4	0.6	0.8	1.0
N_3	0.9051	0.9270	0.9490	0.9710	0.9930	1.0149
$V_{BA}(Cr^{2+})$/eV	1.2173	1.1460	1.0747	1.0033	0.9320	0.8607
$V_{BA}(Co^{2+})$/eV	1.2477	1.1746	1.1015	1.0284	0.9553	0.8822
$V_{BA}(Fe^{2+})$/eV	1.2390	1.1664	1.0938	1.0212	0.9486	0.8760
A site						
Fe^{3+}	0.4396	0.4029	0.3677	0.3341	0.3018	0.2708
Cr^{3+}	0.0000	0.0377	0.0689	0.0939	0.1131	0.1268
Co^{3+}	0.1221	0.0896	0.0614	0.0372	0.0168	0.0000
Fe^{2+}	0.3181	0.3284	0.3387	0.3486	0.3584	0.3680
Cr^{2+}	0.0000	0.0420	0.0865	0.1334	0.1827	0.2343
Co^{2+}	0.1201	0.0993	0.0769	0.0527	0.0271	0.0000
B site						
Fe^{2+}	1.0174	1.0049	0.9898	0.9726	0.9532	0.9320
Cr^{2+}	0.0000	0.0969	0.1909	0.2816	0.3683	0.4507
Co^{2+}	0.6393	0.5014	0.3681	0.2400	0.1172	0.0000
Fe^{3+}	0.2249	0.2637	0.3038	0.3446	0.3865	0.4291
Cr^{3+}	0.0000	0.0234	0.0537	0.0911	0.1359	0.1881
Co^{3+}	0.1184	0.1097	0.0936	0.0701	0.0389	0.0000
$\mu_C/(\mu_B$/formula)	3.2661	3.1200	2.9157	2.6577	2.3508	1.9982

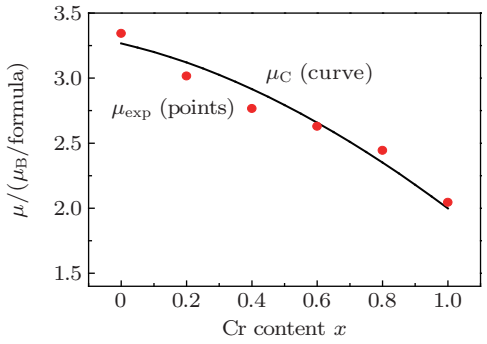


Fig. 6. (color online) Variation of the magnetic moment with Cr-doping concentration x for samples $Co_{1-x}Cr_xFe_2O_4$ $(0.0 \le x \le 1.0)$. Here, the μ_{exp} (points) denotes the experimental magnetic moments, and μ_C (curve) the fitted magnetic moments.

Figure 6 shows the dependence on the Cr-doping level x of the experimental magnetic moment, μ_{exp} (points), and the fitted curve, μ_C (curve). It can be seen that the fitted results are close to the experimental values, which indicates that our assumption concerning the magnetic moment directions of Cr cations is reasonable. Figures 7(a)–7(c) show the curves of the Cr, Co, and Fe cation distributions at the (A) and [B] sites versus x, and figure 7(d) shows the dependences of the distribution of the total numbers of different valence cations per formula on x. It can be seen that the concentration of Cr^{2+} cation at the [B] sites is clearly larger than that of Cr^{3+} at the [B] sites. It can also be seen from Table 3 that the content sum of the Cr^{3+} and Cr^{2+} cations occupying the (A) sites increases from 0.0769 when $x = 0.2$ to 0.3619 when $x = 1.0$, which is similar to the variation trend of the experimental results for the Cr cation distribution obtained by neutron diffraction in $NiCr_xFe_{2-x}O_4$ $(0.0 \le x \le 1.0)$ as reported by Ghatage *et al.*[26] and shown in Fig. 8.

It should be noted that we have used only two independent fitting parameters in the process of fitting the magnetic moments of the six samples $Co_{1-x}Cr_xFe_2O_4$ $(0.0 \le x \le 1.0)$, the values of $V_{BA}(Cr^{2+})$ of the samples for $x = 0.2$ and $x = 0.8$, indicating that our assumptions and fitting method are reasonable.

It should be also noted that we have taken into account the values of ionicity (f_i) of Fe ($f_i = 0.8790$), Cr ($f_i = 0.8726$), and Co ($f_i = 0.8314$) obtained in our previous work.[20] Taking into account the ionicities causes the number of trivalent cations per formula of the samples $Co_{1-x}Cr_xFe_2O_4$ $(0.0 \le x \le 1.0)$, N_3, to increase from 0.9051 for $x = 0.0$ to 1.0149 with $x = 1.0$, as shown in Table 3, rather than to have a constant value of 2.0, as in the traditional view.

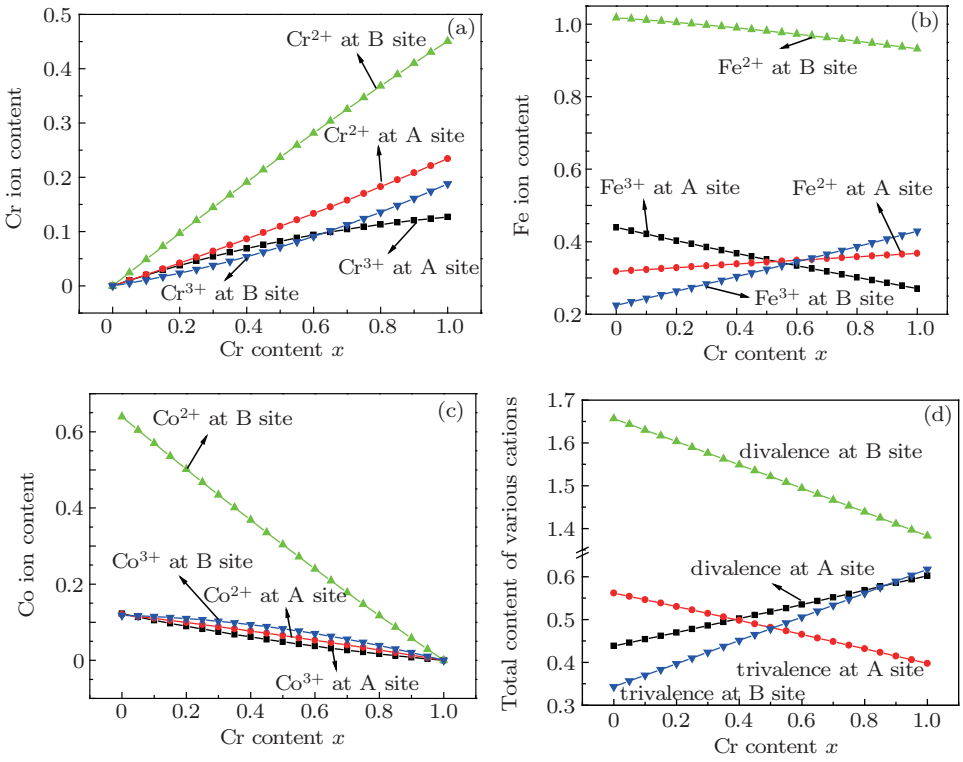


Fig. 7. (color online) Plots of Cr (a), Fe (b), and Co (c) ion content values and the total numbers of divalent and trivalent cations (d) at the (A) and [B] sublattice sites versus Cr-doping level x in the samples $Co_{1-x}Cr_xFe_2O_4$ ($0.0 \leq x \leq 1.0$).

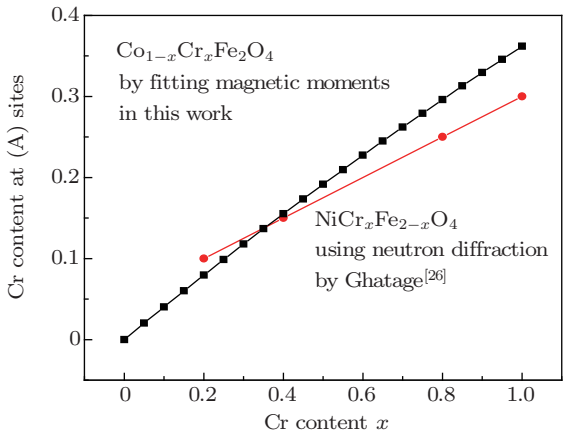


Fig. 8. (color online) Plots of Cr content values at the (A) sites in the samples $Co_{1-x}Cr_xFe_2O_4$, estimated in this work and result for the samples $NiCr_xFe_{2-x}O_4$, obtained from neutron diffraction as reported by Ghatage *et al.*,[26] versus Cr-doped level x.

3.6. Explanation for the variation trend of the lattice constant for the samples $Co_{1-x}Cr_xFe_2O_4$ ($0.0 \leq x \leq 1.0$)

As discussed in Subsection 3.1 and shown in Fig. 2, as the Cr-doped level x increases, the crystal lattice constant decreases when $x < 0.4$, whereas it increases when $x > 0.4$. According to the above cation distributions, this dependence of the lattice constant a on Cr-doping level x can be explained as a competition between the following two factors.

(i) The magnetic moments of Fe and Co cations are parallel, resulting in a magnetic repulsion energy. Because the magnetic moment directions of Cr^{3+} and Cr^{2+} cations are both opposite to the directions of the Fe and Co magnetic moments, doping with Cr will cause the magnetic repulsion energy to reduce and will also cause the lattice constant a to decrease.

(ii) As shown in Subsection 3.1, the observed distance from the O anion to the cations at the (A) sites, d_{AO} is larger than its ideal value, while the observed distance from the O anion to the cations at the [B] sites, d_{BO}, is smaller than its ideal value, implying that the variation of the lattice constant a is mainly determined by d_{AO}. From Fig. 7(d), it can be seen that the total number of divalent cations per formula at the (A) sites increases from 0.424 when $x = 0.0$ to 0.613 when $x = 1.0$, and that the total number of trivalent cations per formula at the (A) sites decreases from 0.576 when $x = 0.0$ to 0.387 when $x = 1.0$. It is known[29] that the effective radii of the divalent cations (0.80, 0.78, and 0.745 Å, respectively, for Cr^{2+}, Fe^{2+}, and Co^{2+} with coordination number six) are significantly larger than those of the corresponding trivalent cations (0.615, 0.645, 0.61 Å). Therefore, the total number of divalent cations per formula at the (A) sites increases, while the total number of trivalent cations decreases, causing the lattice constant of the sample to increase.

It can be seen that the energy corresponding to the factor (i) belongs to the magnetic dipole energy, and that the energy corresponding to the factor (ii) belongs to the Pauli repulsion energy. In general, the magnetic dipole energy is inversely proportional to the distance to the third power, and the Pauli repulsion energy is inversely proportional to the ion distance to the eighth or ninth power. Therefore, the competition be-

tween the two kinds of energies results in the observed nonlinear variation of the lattice constant.

4. Conclusions

Ferrite powder samples of $Co_{1-x}Cr_xFe_2O_4$ ($0.0 \leq x \leq 1.0$) are successfully synthesized using a simple hydrothermal process. The saturation magnetization of the samples decreases as the Cr-doping level x increases. We obtain the cation distributions of the samples by fitting the magnetic moments of the samples at 10 K using the quantum mechanical model that was previously proposed by our group. The calculated sum of the content values of the Cr^{3+} and Cr^{2+} cations occupying (A) sites increases as the value of x increases, which is similar to the variation trend of experimental results for the Cr cation distribution obtained from neutron diffraction in $NiCr_xFe_{2-x}O_4$ ($0.0 \leq x \leq 1.0$) reported by Ghatage *et al*. In the fitting process, the magnetic moment directions of Cr^{3+} and Cr^{2+} cations are assumed to be antiparallel to those of the Fe and Co cations, which is in accordance with Hund's rules. Using this assumption and the estimated cation distribution, the mechanism behind the observation that the lattice constant of the samples decreases as the Cr-doping level x increases when $x < 0.4$, while the lattice constant of the samples increases when $x > 0.4$, which can be clarified.

Acknowledgment

The authors wish to thank Dr. Norm Davison for helpful discussion.

References

[1] Franco A and Silva F C 2010 *Appl. Phy. Lett.* **96** 172505
[2] Zhang R C, Liu L and Xu X L 2011 *Chin. Phys. B* **20** 086101
[3] Wang W J, Zang C G and Jiao Q J 2013 *Chin. Phys. B* **22** 128101
[4] Zhou X, Hou Z L, Li F and Qi X 2010 *Chin. Phys. Lett.* **27** 117501
[5] Liu J H, Zhang L F, Tian G F, Li J C and Li F S 2007 *Acta Phys. Sin.* **56** 6050 (in Chinese)
[6] Jeng H T, Guo G Y and Huang D J 2004 *Phys. Rev. Lett.* **93** 156403
[7] Mohamed R M, Rashad M M, Haraz F A and Sigmund W 2010 *J. Magn. Magn. Mater.* **322** 2058
[8] Chikazumi S 1997 *Physics of Ferromagnetism 2e* (London: Oxford University Press) pp. 150–180
[9] Cojocariu A M, Soroceanu M, Hrib L, Nica V and Caltun O F 2012 *Mater. Chem. Phys.* **135** 728
[10] Chae K P, Lee Y B, Lee J G and Lee S H 2000 *J. Magn. Magn. Mater.* **220** 59
[11] Singhal S, Jauhar S, Singh J, Chandra K and Bansal S 2012 *J. Mol. Struct.* **1012** 182
[12] More S S, Kadam R H, Kadam A B, Shite A R, Mane D R and Jadhav K M 2010 *J. Alloys Compd.* **502** 477
[13] Krieble K, Lo C C H, Melikhov Y and Snyder J E 2006 *J. Appl. Phys.* **99** 08M912
[14] Magalhães F, Pereira M C, Botrel S E C, Fabris J D, Macedo W A, Mendonca R, Lago R M and Oliveira L C A 2007 *Appl. Catal. A-Gen.* **332** 115
[15] Yunus S M, Azad A K, Eriksson S G, Eriksen J, Rundlöf H and Mathieu R 2003 *Physica B* **337** 323
[16] Tang G D, Hou D L, Chen W, Zhao X and Qi W H 2007 *Appl. Phys. Lett.* **90** 144101
[17] Tang G D, Ji D H, Yao Y X, Liu S P, Li Z Z, Qi W H, Han Q J, Hou X and Hou D L 2011 *Appl. Phys. Lett.* **98** 072511
[18] Han Q J, Ji D H, Tang G D, Li Z Z, Hou X, Qi W H, Liu S R and Bian R R 2012 *J. Magn. Magn. Mater.* **324** 1975
[19] Han Q J, Ji D H, Tang G D, Li Z Z, Hou X, Qi W H, Bian R R and Liu S R 2012 *Phys. Status Solidi A* **209** 766
[20] Ji D H, Tang G D, Li Z Z, Hou X, Han Q J, Qi W H, Bian R R and Liu S R 2013 *J. Magn. Magn. Mater.* **326** 197
[21] Phillips J C 1970 *Rev. Mod. Phys.* **42** 317
[22] Liu S R, Ji D H, Xu J, Li Z Z, Tang G D, Bian R R, Qi W H, Shang Z F and Zhang X Y 2013 *J. Alloys Compd.* **581** 616
[23] Ferreira T A S, Waerenborgh J C, Mendonça M H R M, Nunes M R and Costa F M 2003 *Solid State Sci.* **5** 383
[24] Tang G D, Han Q J, Xu J, Ji D H, Qi W H, Li Z Z, Shang Z F and Zhang X Y 2014 *Physica B* **438** 91
[25] Bian R R, Ji D H, Xu J, Li Z Z, Tang G D, Qi W H, Liu S R, Shang Z F and Zhang X Y, in submmision
[26] Ghatage A K, Patil S A and Paranjpe S K 1996 *Solid State Commun.* **98** 885
[27] Rietveld H M 1969 *J. Appl. Cryst.* **2** 65
[28] Chen C W 1977 *Magnetism and Metallurgy of Soft Magnetic Materials* (Amsterdam: North-Holland Publishing Company), pp. 171–417
[29] Shannon R D 1976 *Acta Cryst. A* **32** 751